

Continuum charge excitations in high-valence transition metal oxides revealed by resonant inelastic X-ray scattering

Atsushi Hariki, Mathias Winder, and Jan Kuneš
Institute for Solid State Physics, TU Wien, 1040 Vienna, Austria
(Dated: December 3, 2024)

We present a computational study of Cu L -edge resonant inelastic X-ray scattering (RIXS) of LaCuO_3 and NaCuO_2 , typical high-valence transition-metal oxides, using a theoretical framework based on the local-density approximation + dynamical mean-field theory. This study is motivated by recent experiments, revealing unusual coexistence of bound and continuum excitations in L -edge RIXS spectra. We analyze in detail the behavior of the fluorescence-like (FL) feature and show how it is connected to the details of electronic and crystal structure. On the studied compounds we demonstrate how material details determine whether electron-hole continuum can be excited in the L -edge RIXS process.

Excitation spectrum is a fundamental characteristic that determines properties of a physical system. While the excitations of weakly correlated electrons can be built out of elementary ones and therefore different spectroscopic experiments show the similar spectra, e.g., the same gap for charge, spin and optical excitations, the correlated materials such as transition metal oxides (TMO) are different [1, 2]. Here, the connection between various types of excitations is buried deep in the experimentally unobservable wave function and different techniques are necessary to probe specific excitations.

Following the remarkable improvements of energy resolution in the past decade resonant inelastic X-ray scattering (RIXS) became a popular tool to study diverse materials [3]. Its sensitivity to a range of two-particle excitations enables observation of low-energy spin, orbital and charge excitations (~ 100 meV) [4–7] together with high-energy excitations (~ 1 -10 eV), such as atomic multiplets or charge-transfer (CT) transitions [8–10]. The versatility of RIXS is redeemed by complicated interpretation of the resonant spectra based on theoretical modeling.

Two features have been observed in the L -edge RIXS ($2p \rightarrow 3d \rightarrow 2p$) of TMO when scanning the incident photon energy ω_{in} across the X-ray absorption spectra (XAS): a Raman-like (RL) signal with a constant energy loss $\omega_{\text{loss}} = \omega_{\text{in}} - \omega_{\text{out}}$ and a fluorescence-like (FL) signal with a constant emission energy ω_{out} , i.e., a linear dependence of ω_{loss} on ω_{in} . [3, 9, 11–14]. The analysis of material specific behavior of these features shows a potential for addressing questions concerning itinerancy of charge carriers and localization of charge excitations [12, 14, 15]. While several experimentally motivated interpretations were put forward, a solid theory of the FL feature is missing. The aim of this work is to fill this gap.

The L -edge RIXS spectrum of the CT Mott insulator NiO [8, 9] exhibits a RL behavior at ω_{in} of the main absorption peak well separated from the FL feature at ω_{in} of the CT satellite. A different behavior was reported in the negative-CT compound NdNiO_3 , where Bisogni *et al.* [15] observed merging of the low- ω_{loss} RL and FL features in Ni L_3 -RIXS. Moreover, the details of low- ω_{loss}

FL feature exhibit distinct temperature dependence connected to opening of the charge gap at low temperatures. Bisogni *et al.* interpreted the low- ω_{loss} FL feature as a signature of unbound particle-hole pairs in the final state of RIXS. Zhou *et al.* [12] studied L -edge RIXS in $\text{LaAlO}_3/\text{SrTiO}_3$ heterostructures and interpreted the relative intensity of the FL feature as a measure of concentration of itinerant carriers. This conclusion was recently questioned by Pfaff *et al.* [14] who suggested that either RL or FL signals reflects the nature of the intermediate state of the RIXS process.

Theoretical description of RIXS in high-valence TMO is a challenging task. The commonly used cluster model with the TM $3d$ and the neighboring O $2p$ orbitals misses the FL feature completely due the lack of continuum (delocalized) particle-hole excitations. This is remedied by the Anderson impurity model (AIM), however, the use of simple model bath densities of states [8–10, 15] does not allow to capture the important material details. To overcome this limitation we employ the local-density approximation (LDA) + dynamical mean-field theory (DMFT) [16, 17] approach. The AIM with material specific hybridization density is then extended to include the core orbitals [18]. This approach, which we recently applied to study the non-local screening effects in L -edge X-ray photoemission spectroscopy (XPS) [18], is here extended to analyze RIXS.

We choose the isoelectronic Cu^{3+} compounds LaCuO_3 and NaCuO_2 as model systems of high-valence TMO. Both share a tiny CT energy [19–23] leading to small or no gap [19, 21, 22, 24, 25]. As we show later the key difference between the two compounds is the lattice geometry with corner-sharing CuO_6 octahedra in LaCuO_3 , but edge-sharing ones in NaCuO_2 , see Fig. 1.

The calculations proceed in two steps. First, the LDA calculation was performed using the Wien2K package [27] in $P4/m$ tetragonal and $C2/m$ monoclinic structure for LaCuO_3 [24] and NaCuO_2 [28], respectively. Then, a dp tight-binding model spanning the Cu $3d$ and O $2p$ orbitals is constructed [29, 30] and augmented with the electron-electron interaction within the Cu $3d$ shell giving

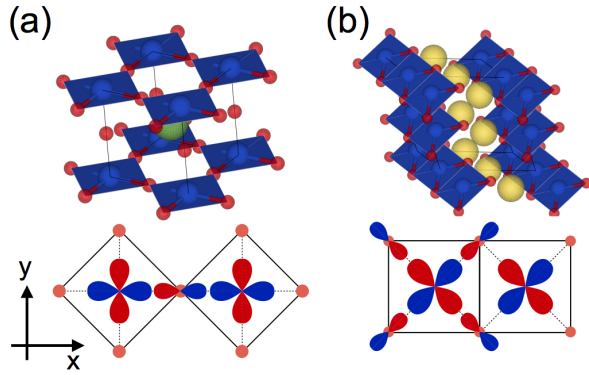


FIG. 1. (Color online) The crystal structure of (a) LaCuO_3 and (b) NaCuO_2 visualized by VESTA [26]. The blue, red and green, yellow circles represent Cu, O, La and Na atoms, respectively. The sketch of the xy plane is shown together.

the Hamiltonian

$$H = \sum_{\mathbf{k}} (\mathbf{d}_{\mathbf{k}}^{\dagger} \mathbf{p}_{\mathbf{k}}^{\dagger}) \begin{pmatrix} h_{\mathbf{k}}^{dd} - \mu_{dc} & h_{\mathbf{k}}^{dp} \\ h_{\mathbf{k}}^{pd} & h_{\mathbf{k}}^{pp} \end{pmatrix} \begin{pmatrix} \mathbf{d}_{\mathbf{k}} \\ \mathbf{p}_{\mathbf{k}} \end{pmatrix} + \sum_i W_i^{dd}.$$

Here, $\mathbf{d}_{\mathbf{k}}^{\dagger} (\mathbf{p}_{\mathbf{k}}^{\dagger})$ is an operator-valued vector whose elements are Fourier transforms of $d_{\alpha i} (p_{\gamma i})$, that annihilate the Cu 3d (O 2p) electron in the orbital α (γ) in the i -th unit cell. The on-site Coulomb interaction W_i^{dd} is approximated by the density-density form with parameters $U = 7.5$ eV and $J = 0.98$ eV, which are typical values for Cu systems [31]. The double-counting term μ_{dc} , which corrects for the d - d interaction present in the LDA step, renormalizes the p - d splitting and thus the CT energy. We have treated μ_{dc} as adjustable parameter, see Supplementary material (SM), and fixed its value by comparison to available L -edge XAS and valence XPS data. The continuous-time quantum Monte Carlo method with the hybridization expansion [32–34] was used to solve the auxiliary AIM.

In Fig. 2a,b we show the one-particle spectral functions of LaCuO_3 and NaCuO_2 calculated by LDA+DMFT. The $\mu_{dc} = 56.64 \pm 1$ eV yields results consistent with earlier valence and Cu L -edge XAS studies [19, 21]. For LaCuO_3 , paramagnetic metal (PM) and antiferromagnetic insulator (AFI) solutions can be stabilized, similar to LDA+ U studies [22], indicating the Slater-nature of the gap. Reflecting the unclear experimental situation [21, 22, 24, 25], we proceed with both states and use them later to demonstrate the effect of the small gap on RIXS. NaCuO_2 ($E_{\text{gap}} \approx 0.5$ eV) has a band-insulator character with a gap present already in the LDA solution [35, 36]. Overall, the spectral functions suggest existing phase space for continuum of p - p excitations in the few eV range.

In the second step, we compute the RIXS spectra of AIM with Cu 2p core states and DMFT hybridization density [18]. The RIXS intensity at finite temperature T

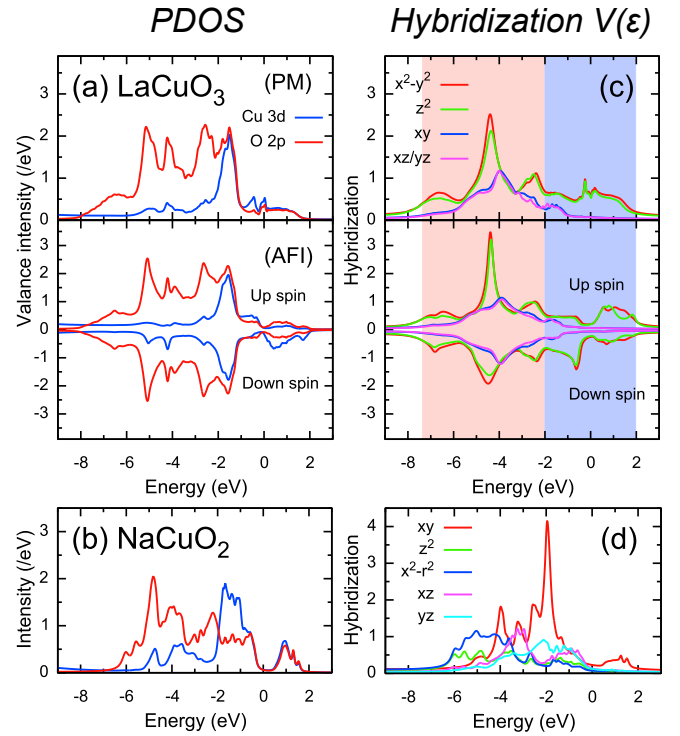


FIG. 2. (Color online) LDA+DMFT valence intensity of (a) LaCuO_3 in the PM and AFI phases and (b) NaCuO_2 . The hybridization function of (c) LaCuO_3 in the PM and AFI phases and (d) NaCuO_2 . The energy origin is taken at E_F .

is described by [9, 10, 37]

$$F_{\text{RIXS}}(\omega_{\text{out}}, \omega_{\text{in}}) = \sum_n F_{\text{RIXS}}^{(n)}(\omega_{\text{out}}, \omega_{\text{in}}) e^{-E_n/k_B T} / Z,$$

where

$$\begin{aligned} F_{\text{RIXS}}^{(n)}(\omega_{\text{out}}, \omega_{\text{in}}) &= \sum_f \left| \sum_m \frac{\langle f | T_e | m \rangle \langle m | T_i | n \rangle}{\omega_{\text{in}} + E_n - E_m + i\Gamma_L} \right|^2 \\ &\times \delta(\omega_{\text{in}} + E_n - \omega_{\text{out}} - E_f) \\ &= \sum_f \left| \langle f | T_e \frac{1}{\omega_{\text{in}} + E_n - H_{\text{imp}} + i\Gamma_L} T_i | n \rangle \right|^2 \\ &\times \delta(\omega_{\text{in}} + E_n - \omega_{\text{out}} - E_f) \end{aligned} \quad (1)$$

Here $|n\rangle$, $|m\rangle$ and $|f\rangle$ are the initial, intermediate and final states with energies E_n , E_m and E_f , respectively, and $e^{-E_n/k_B T} / Z$ is the Boltzmann factor with the partition function Z . Γ_L is the lifetime width of the intermediate state, and T_i (T_e) describes the dipole transition for the incident (emitted) photon. H_{imp} is the AIM Hamiltonian augmented by the core orbitals and their interaction with Cu 3d orbitals, see Eq. (3) in Ref. [18]. In the actual calculation the resolvent formulation on the second line of (1) is used. The configuration interaction scheme [18] with 25 bath states representing the DMFT

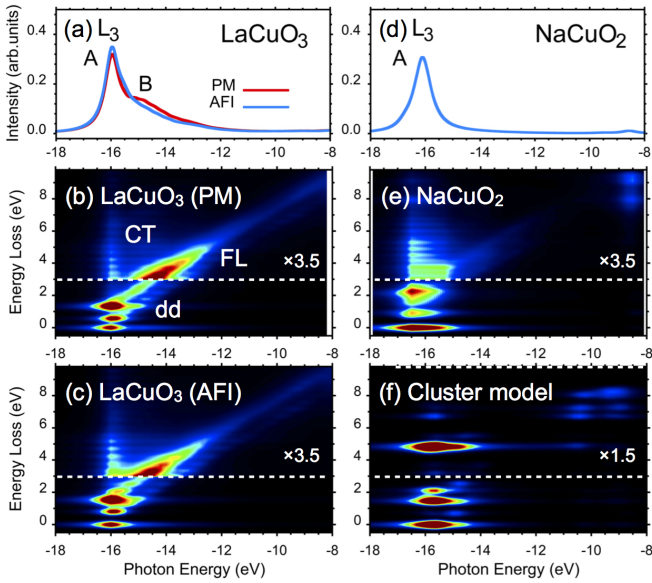


FIG. 3. (Color online) (a)-(e) the calculated L -edge XAS and RIXS for LaCuO_3 in PM and AFI phase (left) and NaCuO_2 (right). The RIXS intensity with $\omega_{\text{loss}} \geq 3.0$ eV (dashed line) are magnified by 3.5 times. (f) the calculated RIXS by the CuO_6 cluster model. The spectral broadening is considered using a Gaussian of 150 meV for RIXS and a Lorentzian 300 meV for XAS (HWHM).

hybridization density is employed to evaluate Eq. (1). We also compute L -edge XAS spectra since the intermediate state $|m\rangle$ (corresponding to the final state of XAS) provides an important clue for interpretation of L -edge RIXS spectra. Details of the calculation can be found in SM.

The calculated Cu L_3 -edge XAS and RIXS spectra are shown in Fig. 3. The XAS spectrum of NaCuO_2 has a single-peak (A), while that of LaCuO_3 exhibits an additional shoulder (B), enhanced in PM phase, observed also in experiment [21]. The shoulder B is missing in the calculations on the CuO_6 cluster model [21, 38], indicating that the shoulder is not of d - d or CT origin but due to a final state delocalized beyond the CuO_6 cluster. Such a nonlocal charge excitation is captured by the present approach [18].

The RIXS spectra of NaCuO_2 and LaCuO_3 are strikingly different. Tuning ω_{in} to the peak A of XAS, two distinct d - d transitions with RL behavior are found in both compounds, similar to another Cu^{3+} material $\text{Zn}_{1-x}\text{Cu}_x\text{O}$ [39], followed by CT transitions with higher ω_{loss} . However, at higher ω_{in} the RIXS of LaCuO_3 yields a linear FL feature, with little difference between the AFI and PM phase. The FL feature is suppressed in NaCuO_2 resembling the spectrum of the cluster model in Fig. 3f. The calculated RIXS spectra of LaCuO_3 remind of the experimental observation on NdNiO_3 [15] with the FL feature starting at the ω_{in} on the L_3 main-edge and not far above it as in NiO . The continuum of unbound

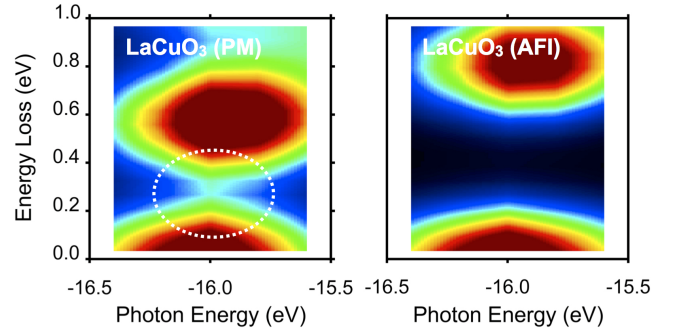


FIG. 4. (Color online) Magnification of the low energy loss region (< 1.0) of RIXS map in PM and AFI phases of LaCuO_3 . The FL feature continues to zero energy loss ω_{loss} in the PM phase.

particle-hole pairs *à la* Ref. [15] explains the FL feature in LaCuO_3 .

Why is the FL feature missing in NaCuO_2 then? The small NaCuO_2 gap cannot explain the absence of visible particle-hole excitations at ω_{loss} in the 3-4 eV range. In fact, the experiment on NdNiO_3 [15] and the calculations in the PM and AFI phases of LaCuO_3 in Fig. 4 show that the gap opening affects the FL feature only at low ω_{loss} . Moreover, the NaCuO_2 spectral function, Fig. 2b, exhibits noticeably higher density of states above and below the gap than LaCuO_3 , Fig. 2a, suggesting a larger phase space for particle-hole excitations. To answer this question we show, in Figs. 2c,d, the hybridization intensities

$$V^2(\varepsilon) = \sum_{\alpha} \frac{V_{\alpha}^2}{\varepsilon - \varepsilon_{\alpha}},$$

which describe how a given Cu atom orbital hybridizes with the rest of the crystal. Here, V_{α} is the hopping amplitude between the Cu ion and auxiliary orbitals at energies ε_{α} [40], which represent the effect of the nearest-neighbor oxygen ligands as well as the more distant atoms [16, 18]. It is instructive to consider the $V(\varepsilon)$ of the cluster model first. Here, $V(\varepsilon)$ is a single Dirac δ -function peaked at the energy ε_p of the unhybridized ligand orbital, while the O $2p$ spectral function exhibits two peaks corresponding to the bonding and anti-bonding states.

A prominent peak in $V(\varepsilon)$ (for e_g orbitals) due to hybridization to nearest-neighbor O ligands is found in both LaCuO_3 and NaCuO_2 , see Figs. 2c,d. The continuum part of $V(\varepsilon)$ in the two materials reveals a substantial difference. While in LaCuO_3 a substantial hybridization intensity exists in the low-energy region of -2 to 2 eV (see blue shadow in the figure), the $V(\varepsilon)$ of NaCuO_2 resembles that of the cluster model with a weak continuum background. This is how the local quantity $V(\varepsilon)$, relevant for description of the core-level excitation, encodes the information about bonding and lattice geometry. In LaCuO_3 , the corner-sharing network of CuO_6 octahedra

allows electrons/holes to propagate through the strong Cu-O σ -bonds and thus gives rise to the continuum of $V(\varepsilon)$. This is not possible in the chains of edge sharing CuO_4 plaquettes in NaCuO_2 , where the neighboring Cu ions form σ -bonds with orthogonal O $2p$ orbitals, see Fig. 1, and the crystal resembles a collection of weakly coupled CuO_4 clusters.

How does the hybridization intensity affect the RIXS spectra? In Eq. (1), all intermediate states accessible in the XAS process contribute to RIXS in principle. We estimate that the intermediate states with $|E_m - E_n - \omega_{\text{in}}| \lesssim \Gamma_L$, which approximately conserve energy in the partial XAS process, dominate while those outside this range cancel approximately out due to the varying sign of the denominator. Such a claim cannot be directly confirmed with the resolvent formulation of Eq. (1). It is, nevertheless, supported by the diagonal shape of the FL feature in the $\omega_{\text{in}}-\omega_{\text{loss}}$ plane, suggesting that a narrow range of intermediate states are 'excited' that 'decay' into narrow range of final states with matching electron-hole excitation. The small hybridization intensity for $\varepsilon > 0$ in NaCuO_2 implies that (intermediate) states with different number of conduction electrons hybridize only weakly with one another. In LaCuO_3 a RIXS process that we schematically write as $d^8 + d^9 \underline{v} \rightarrow \underline{C}d^{10} \underline{v} + \underline{C}d^9 \underline{c} \underline{v} \rightarrow d^8 \underline{c} \underline{v}$ ends up in a final state that can be characterized as the ground state plus an electron-hole pair in the continuum, see Fig 5d, where \underline{C} , \underline{v} and \underline{c} correspond to a hole in $2p$ core-level, in valence bands and an electron in conduction bands, respectively. Such processes in NaCuO_2 are strongly suppressed since states of the type $\underline{C}d^{10} \underline{v}$ and $\underline{C}d^9 \underline{c} \underline{v}$ hybridize only weakly. This is a local expression of the fact that in NaCuO_2 a hole transferred from Cu to O has a small probability to escape the CuO_4 cluster.

To test this interpretation, we have switched off the hybridization to the conduction band in the intermediate states for the PM phase of LaCuO_3 , see Fig. 5bc, i.e., we have set $V(\varepsilon > 0) = 0$ in the H_{imp} of Eq. 1 while keeping the initial and final states corresponding to unrestricted $V(\varepsilon)$ unchanged. The intensity of the FL feature is dramatically suppressed and resembles that of NaCuO_2 or cluster model. Although (unchanged) final states with excited electron-hole pairs exist, they cannot be resonantly excited by the RIXS process. Cutting hybridization to the conduction states affects also the XAS spectrum, see Fig. 5a, which loses the shoulder B and overlaps with that of the cluster model. This shows that intermediate states with localized and delocalized character coexist in this ω_{in} -region, which leads to coexistence of the FL and RL features in RIXS spectrum.

In summary, we have studied the coexistence of RL and FL features in two typical high valence transition metal oxides LaCuO_3 and NaCuO_2 . While a phase space for particle-hole excitations with mixed Cu $3d$ -O $2p$ exists in both compounds, only the RIXS spectrum of LaCuO_3

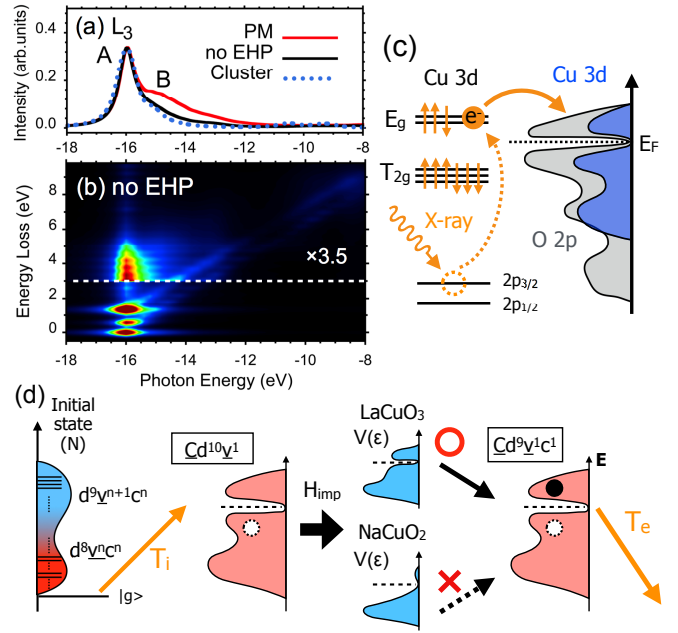


FIG. 5. (Color online) The calculated L -edge (a) XAS and (b) RIXS for LaCuO_3 in PM phase in which the CT to the conduction states above E_F is removed *only* in the intermediate state (denoted as “no EHP”). (c) Schematic of CT to the conduction states in the intermediate state. (d) Schematic of electron-hole pair creation in RIXS process.

hosts the FL feature. We have shown that for geometrical reasons the unbound electron-hole excitations responsible for the FL feature cannot be excited by the RIXS process in NaCuO_2 . This fact is captured by the hybridization intensity of the Anderson impurity model, which provides the local description of RIXS. Moreover, we have shown that the low- ω_{loss} FL feature is sensitive to the opening of a small gap similar to the experimental observation on NdNiO_3 [15]. The present results show that FL component of the RIXS spectra is rather material specific, however, its interpretation requires advanced many-body calculations.

The authors thank R. Claessen, M. Sing, P. Scheiderer, T. Uozumi, R.-P. Wang, A. Sotnikov and J. Fernández Afonso for fruitful discussions. The authors are supported by the European Research Council (ERC) under the European Union’s Horizon 2020 research and innovation programme (grant agreement No. 646807-EXMAG). The computational calculations were performed at the Vienna Scientific Cluster (VSC).

- [1] M. Imada, A. Fujimori, and Y. Tokura, *Rev. Mod. Phys.* **70**, 1039 (1998).
- [2] D. I. Khomskii, *Transition Metal Compounds* (Cambridge University Press, 2014).
- [3] L. J. P. Ament, M. van Veenendaal, T. P. Devereaux,

- J. P. Hill, and J. van den Brink, *Rev. Mod. Phys.* **83**, 705 (2011).
- [4] D. Betto, Y. Y. Peng, S. B. Porter, G. Berti, A. Calloni, G. Ghiringhelli, and N. B. Brookes, *Phys. Rev. B* **96**, 020409 (2017).
- [5] G. Fabbris, D. Meyers, L. Xu, V. M. Katukuri, L. Hozoi, X. Liu, Z.-Y. Chen, J. Okamoto, T. Schmitt, A. Uldry, B. Delley, G. D. Gu, D. Prabhakaran, A. T. Boothroyd, J. van den Brink, D. J. Huang, and M. P. M. Dean, *Phys. Rev. Lett.* **118**, 156402 (2017).
- [6] J. Kim, D. Casa, M. H. Upton, T. Gog, Y.-J. Kim, J. F. Mitchell, M. van Veenendaal, M. Daghofer, J. van den Brink, G. Khaliullin, and B. J. Kim, *Phys. Rev. Lett.* **108**, 177003 (2012).
- [7] L. Braicovich, L. J. P. Ament, V. Bisogni, F. Forte, C. Aruta, G. Balestrino, N. B. Brookes, G. M. De Luca, P. G. Medaglia, F. M. Granozio, M. Radovic, M. Saluzzo, J. van den Brink, and G. Ghiringhelli, *Phys. Rev. Lett.* **102**, 167401 (2009).
- [8] G. Ghiringhelli, M. Matsubara, C. Dallera, F. Fracassi, R. Gusmeroli, A. Piazzalunga, A. Tagliaferri, N. B. Brookes, A. Kotani, and L. Braicovich, *J. Phys. Condens. Matter* **17**, 5397 (2005).
- [9] M. Matsubara, T. Uozumi, A. Kotani, and J. C. Parlebas, *J. Phys. Soc. Jpn.* **74**, 2052 (2005).
- [10] F. de Groot and A. Kotani, *Core Level Spectroscopy of Solids* (CRC Press, 2014).
- [11] A. Kotani and S. Shin, *Rev. Mod. Phys.* **73**, 203 (2001).
- [12] K.-J. Zhou, M. Radovic, J. Schlappa, V. Strocov, R. Frison, J. Mesot, L. Patthey, and T. Schmitt, *Phys. Rev. B* **83**, 201402 (2011).
- [13] T. Schmitt, L.-C. Duda, M. Matsubara, M. Mattesini, M. Klemm, A. Augustsson, J.-H. Guo, T. Uozumi, S. Horn, R. Ahuja, A. Kotani, and J. Nordgren, *Phys. Rev. B* **69**, 125103 (2004).
- [14] F. Pfaff, H. Fujiwara, G. Berner, A. Yamasaki, H. Niwa, H. Kiuchi, A. Gloskovskii, W. Drube, J. Gabel, O. Kirilmaz, A. Sekiyama, J. Miyawaki, Y. Harada, S. Suga, M. Sing, and R. Claessen, *Phys. Rev. B* **97**, 035110 (2018).
- [15] V. Bisogni, S. Catalano, R. J. Green, M. Gibert, R. Scherwitzl, Y. Huang, V. N. Strocov, P. Zubko, S. Balandeh, J.-M. Triscone, G. Sawatzky, and T. Schmitt, *Nat Commun.* **7**, 13017 (2016).
- [16] G. Kotliar, S. Y. Savrasov, K. Haule, V. S. Oudovenko, O. Parcollet, and C. A. Marianetti, *Rev. Mod. Phys.* **78**, 865 (2006).
- [17] A. Georges, G. Kotliar, W. Krauth, and M. J. Rozenberg, *Rev. Mod. Phys.* **68**, 13 (1996).
- [18] A. Hariki, T. Uozumi, and J. Kuneš, *Phys. Rev. B* **96**, 045111 (2017).
- [19] T. Mizokawa, H. Namatame, A. Fujimori, K. Akeyama, H. Kondoh, H. Kuroda, and N. Kosugi, *Phys. Rev. Lett.* **67**, 1638 (1991).
- [20] D. Khomskii, eprint arXiv:cond-mat/0101164 (2001), cond-mat/0101164.
- [21] T. Mizokawa, A. Fujimori, H. Namatame, Y. Takeda, and M. Takano, *Phys. Rev. B* **57**, 9550 (1998).
- [22] M. T. Czyżyk and G. A. Sawatzky, *Phys. Rev. B* **49**, 14211 (1994).
- [23] T. Mizokawa, A. Fujimori, H. Namatame, K. Akeyama, and N. Kosugi, *Phys. Rev. B* **49**, 7193 (1994).
- [24] J. F. Bringley, B. A. Scott, S. J. La Placa, T. R. McGuire, F. Mehran, M. W. McElfresh, and D. E. Cox, *Phys. Rev. B* **47**, 15269 (1993).
- [25] S. Darracq, S. Matar, and G. Demazeau, *Solid State Commun* **85**, 961 (1993).
- [26] K. Momma and F. Izumi, *Journal of Applied Crystallography* **44**, 1272 (2011).
- [27] P. Blaha, K. Schwarz, G. Madsen, D. Kvasnicka, and J. Luitz, *WIEN2k, An Augmented Plane Wave + Local Orbitals Program for Calculating Crystal Properties (Karlheinz Schwarz, Techn. Universitat Wien, Austria, 2001)*, ISBN 3-9501031-1-2.
- [28] N. E. Brese, M. O’Keeffe, R. B. V. Dreele, and V. G. Young, *Journal of Solid State Chemistry* **83**, 1 (1989).
- [29] J. Kuneš, R. Arita, P. Wissgott, A. Toschi, H. Ikeda, and K. Held, *Comput. Phys. Commun.* **181**, 1888 (2010).
- [30] A. A. Mostofi, J. R. Yates, G. Pizzi, Y.-S. Lee, I. Souza, D. Vanderbilt, and N. Marzari, *Comput. Phys. Commun.* **185**, 2309 (2014).
- [31] V. I. Anisimov, J. Zaanen, and O. K. Andersen, *Phys. Rev. B* **44**, 943 (1991).
- [32] P. Werner, A. Comanac, L. de’ Medici, M. Troyer, and A. J. Millis, *Phys. Rev. Lett.* **97**, 076405 (2006).
- [33] L. Boehnke, H. Hafermann, M. Ferrero, F. Lechermann, and O. Parcollet, *Phys. Rev. B* **84**, 075145 (2011).
- [34] H. Hafermann, K. R. Patton, and P. Werner, *Phys. Rev. B* **85**, 205106 (2012).
- [35] D. J. Singh, *Phys. Rev. B* **49**, 1580 (1994).
- [36] D. Choudhury, P. Rivero, D. Meyers, X. Liu, Y. Cao, S. Middey, M. J. Whittaker, S. Barraza-Lopez, J. W. Freeland, M. Greenblatt, and J. Chakhalian, *Phys. Rev. B* **92**, 201108 (2015).
- [37] H. A. Kramers and W. Heisenberg, *Zeitschrift für Physik* **31**, 681 (1925).
- [38] K. Okada and A. Kotani, *J. Phys. Soc. Jpn* **68**, 666 (1999).
- [39] P. Thakur, V. Bisogni, J. C. Cezar, N. B. Brookes, G. Ghiringhelli, S. Gautam, K. H. Chae, M. Subramanian, R. Jayavel, and K. Asokan, *J. Appl. Phys.* **107**, 103915 (2010).
- [40] In both materials an independent set of α -orbitals can be, to a good approximation, chosen for each Cu orbital.